Retarding field analyzer for the EAST plasma boundary

Y. L. Li, G. S. Xu, C. Xiao, H. Q. Wang, N. Yan, B. N. Wan, L. Chen, Y. L. Liu, H. Zhang, W. Zhang, L. Wang, G. H. Hu, R. Chen, J. C. Xu, Y. Ye, and J. Li

Citation: Review of Scientific Instruments **87**, 123503 (2016); doi: 10.1063/1.4971317
View online: http://dx.doi.org/10.1063/1.4971317
View Table of Contents: http://aip.scitation.org/toc/rsi/87/12
Published by the American Institute of Physics

Retarding field analyzer for the EAST plasma boundary

Y. L. Li,[1] G. S. Xu,[1] C. Xiao,[1,2] H. Q. Wang,[1] N. Yan,[1] B. N. Wan,[1] L. Chen,[1] Y. L. Liu,[1] H. Zhang,[1] W. Zhang,[1] L. Wang,[1] G. H. Hu,[1] R. Chen,[1] J. C. Xu,[1] Y. Ye,[1] and J. Li[1]
[1]*Institute of Plasma Physics, Chinese Academy of Sciences, Hefei 230031, People's Republic of China*
[2]*Department of Physics and Engineering Physics, University of Saskatchewan, 116 Science Place, Saskatoon, Saskatchewan S7N 5E2, Canada*

(Received 21 July 2016; accepted 19 November 2016; published online 8 December 2016)

A novel bi-directional Retarding Field Analyzer (RFA) probe has been installed on a fast reciprocating drive system on the Experimental Advanced Superconducting Tokamak (EAST) to measure the ion temperature and fast electron fluxes. A Langmuir probe assembly was added on the top of the RFA head to control the RFA position relative to the last closed flux surface and to have a possibility to measure the electron density and temperature as well. Except the ion temperature, the fast electron fluxes from both ion and electron drift sides have been measured during lower hybrid current drive. The RFA probe has been also used to measure the fast electrons associated with edge localized modes (ELMs), indicating their substantial presence in the scrape-off-layer plasma of EAST. *Published by AIP Publishing.* [http://dx.doi.org/10.1063/1.4971317]

I. INTRODUCTION

The Retarding Field Analyzer (RFA) is essentially the only practical tool to measure the ion temperature in the tokamak boundary plasmas.[1] Recently, the alternative Ion Sensitive Probe (ISP) technique turned out to be inaccurate to measure the ion temperature due to the space-charge limitation.[2] To date, RFA has been used on JET,[3] Tore Supra,[4] Alcator C-mod,[5] ISTTOK,[6] STOR-M,[7] HL-2A[8] tokamaks, and other plasma devices to measure the edge ion temperature profile. Generally, the RFA consists of an input slit, two or three grids, and a collector. One of the grids is biased positively to repel plasma ions entering into the RFA cavity through the entrance slit. The conventional RFA application is based on the RFA collector current and the grid repelling voltage (I-V) characteristic and an RFA model of shifted Maxwellian distribution of the ions. The I-V curve is then fitted to an exponential function to extract the ion temperature T_i. Usually the entrance slit of an RFA is negatively biased to repel the plasma electrons and let only the ions to enter the RFA cavity. However, during the Lower Hybrid Current Drive (LHCD) operation, fast electrons can overcome the entrance slit potential and arrive at the RFA collector completely swamping the ion current, as has been observed on the Tore Supra tokamak.[9,10]

This paper describes the Experimental Advanced Superconducting Tokamak (EAST) bi-directional RFA and presents the measurements of ion temperature and fast electron fluxes from both ion and electron drift sides. In Section II the principle and design of the RFA are described. Experimental results are presented in Section III, while Section IV summarizes the paper.

II. RFA

A. RFA principle

The measured RFA current depends on the retarding voltage and the ion distribution function through the following formula:[4]

$$I_C = A_{slit} e Z \int_{\sqrt{2eZV_1/m_i}}^{\infty} \xi_{total} v_{\parallel} f(v_{\parallel}) dv_{\parallel}, \tag{1}$$

where I_c is the RFA collector current, A_{slit} is the area of entrance slit, e is the electron charge, m_i is the ion mass, Z is the ion charge number, V_1 is the retarding voltage, ξ_{total} is the total ion transmission coefficient, and $f(v_{\parallel})$ is the ion distribution function for the velocities parallel to the magnetic field line. Assuming that the ion velocity distribution function is Maxwellian, Eq. (1) can be simplified as

$$I_C = \begin{cases} I_0, & V_1 < V_s \\ I_0 e^{-(V_1 - V_s)Z/T_i}, & V_1 \geq V_s \end{cases}, \tag{2}$$

where I_0 is the maximum ion current when no ions are repelled by the retarding potential V_1 and V_s is the potential difference between the plasma and the entrance slit plate.

In accordance with Eq. (2), the ion temperature is obtained from the RFA experimental I-V characteristic fitted by four parametric (a, b, c, and d) functions,

$$I = a \times \exp(b \times (V_G - c)) + d, \tag{3}$$

where I and V_G are, respectively, the collected current and scanning voltage, and the parameter b is $b = T_i/Z_i$, where Z_i is the ion charge number (for pure deuterium plasma $Z_i = 1$). In Ref. 11, the influence of the impurity ions was studied by simulating the measurements of an RFA exposed to a mixture of impurity and fuel ion fluxes. The result showed that the assumption of plasma purity caused T_i to be underestimated by as much as ~20%.

I_0 in Eq. (2) satisfies the formula

$$I_0 = A_{slit} e \Gamma_{in} \xi_r (1 - \xi)^2, \tag{4}$$

where Γ_{in} is the incident ion flux and ξ is the absorption coefficient of the grids for the ions. $\xi_r = \Gamma_{tr}/\Gamma_{in}$ is the slit relative transmission factor given by the ratio of the transmitted flux Γ_{tr} to the incoming flux Γ_{in}. In order to obtain the value of ξ_r,

three assumptions have been made: (a) the parallel ion velocity distribution is shifted in the Maxwellian velocity distribution $f(v_x, v_y, v_z) = C\exp(\frac{m}{2kT}[(v_x - v_0)^2 + v_y^2 + v_z^2])$, where v_0 is the flow velocity due to acceleration of ions between the plasma and the entrance slit; (b) the magnetic field is parallel to the RFA cavity axis; (c) the error function is approximated to be $erf(c \cdot x) = \frac{2}{\sqrt{\pi}}\int_0^{cx} e^{-t^2}dt \approx 1 - \exp(-1.842c \cdot x)$. Based on assumption (a), the incident ion flux Γ_{in} could be integrated according to the following formula:

$$\Gamma_{in} = \int_0^{\infty} v_x dv_x \int_{-\infty}^{\infty} dv_y \int_{-\infty}^{\infty} dv_z f(v_x, v_y, dv_z) = \frac{\pi}{2}\left(\frac{2kT_i}{m_i}\right)^2 \{\exp(-M^2) + \sqrt{\pi}M[1 + erf(M)]\}, \quad (5)$$

where $M = v_0\sqrt{m/2kT}$ is the Mach number. Using assumption (b), the transmitted ion flux Γ_{tr} could be expressed by the following formula:

$$\Gamma_{tr} = \int_0^{\infty} v_x dv_x \int_{-\infty}^{\infty} dv_y \int_{-v_x w/2s}^{v_x w/2s} dv_z f(v_x, v_y, dv_z) = \pi\left(\frac{2kT_i}{m_i}\right)^2 \left\{(\frac{a\sqrt{\pi}}{4} - \frac{\sqrt{\pi}M}{2})\exp(\frac{a^2}{4} - a \cdot M)erfc(\frac{a}{2} - M) + \frac{\sqrt{\pi}M}{2}[1 + erf(M)]\right\}, \quad (6)$$

where $erfc(x) = 1 - erf(x)$ is the co-error function, and the integration range for v_z is limited by the ratio of the slit width and depth. The parameter $a = 1.842 \times (w/2s)$. Assumption (c) has been used to analytically solve the integral. Then ξ_r can be solved as a function of M and a,

$$\xi_r = \frac{(0.5 \times a\sqrt{\pi} - \sqrt{\pi}M)\exp(\frac{a^2}{4} - a \cdot M)erfc(\frac{a}{2} - M) + \sqrt{\pi}M[1 + erf(M)]}{\exp(-M^2) + \sqrt{\pi}M[1 + erf(M)]}. \quad (7)$$

The dependences of ξ_r on w/2s and M are shown in Fig. 1(b). According to this figure, ξ_r increases significantly with w/2s and slightly with the Mach number. With a known ξ_r value and other parameters in Eq. (4), the collector current I_0 can be calculated. During the RFA design, I_0 should be smaller than the space charge limited current, I_{SCL}, to ensure that the collector current satisfies Eq. (2). Generally, in the space charge limit regime, the current density between the two infinite parallel plate electrodes is limited due to potential hill established by the charge distributed between the electrodes. This space charge limited current is expressed by the Child-Langmuir formula,[12]

$$I_{\mathrm{SCL}} = \frac{4}{9}\varepsilon_0\sqrt{\frac{2e}{m_i}}\frac{S}{d^2}V^{3/2}, \quad (8)$$

where ε_0 is the permittivity of the free space, S is the ion flux area, and d and V are the spacing and voltage between the grids. The currents I_{SCL} and I_0 are compared in Section II B.

B. RFA head design

The RFA consists of an entrance slit, two successive grids (biased, respectively, by a positive scanning voltage, and negative voltage to suppress secondary electrons from the collector), and the collector plate. More details of the EAST bidirectional RFA head are presented in Fig. 2, showing the tubular spacer rings, central spacer, Langmuir probe pins, electrical contact rings, cavity, and graphite shield. The tungsten (99.95% of purity) entrance slit was purchased from Gateway Laser Services, Inc.[13] Three parallel narrow entrance slits were designed to increase the current collected by the collector plate. The plasma sheath continuity across the slit requires the entrance slit width, w, to be 1-2 times the Debye length $\lambda_D = \sqrt{\varepsilon_0 T_e/(n_e e^2)}$. λ_D in the EAST scrape-off-layer (SOL) plasma region is about 15-50 μm for different regimes. The width, w, and thickness, s, of the slit have

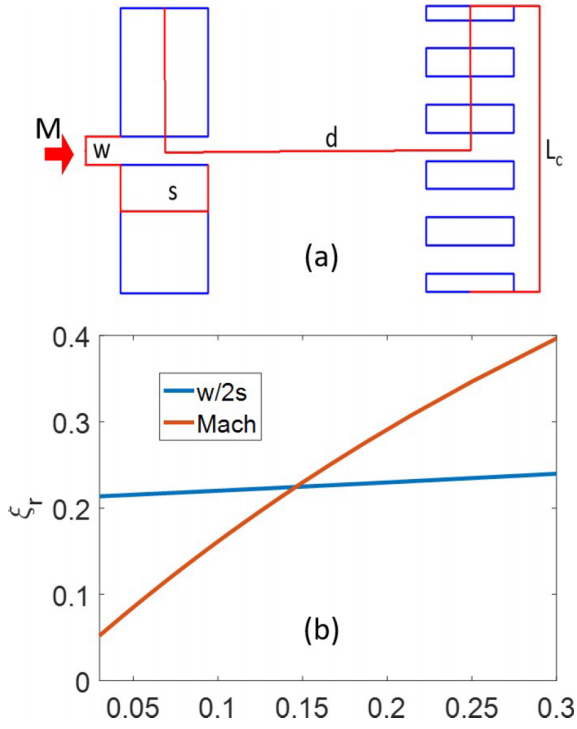

FIG. 1. (a) Schematic diagram of the entrance slit and the first grid where the z axis is along the magnetic field, the slit width w along the x axis, the slit height along the y axis. The symbol s indicates the slit thickness, d the distance between the slit and the grid, Lc the grid diameter, M the Mach number. (b) Transmission factor of the entrance slit varying with the slit parameter w/2s and M, respectively.

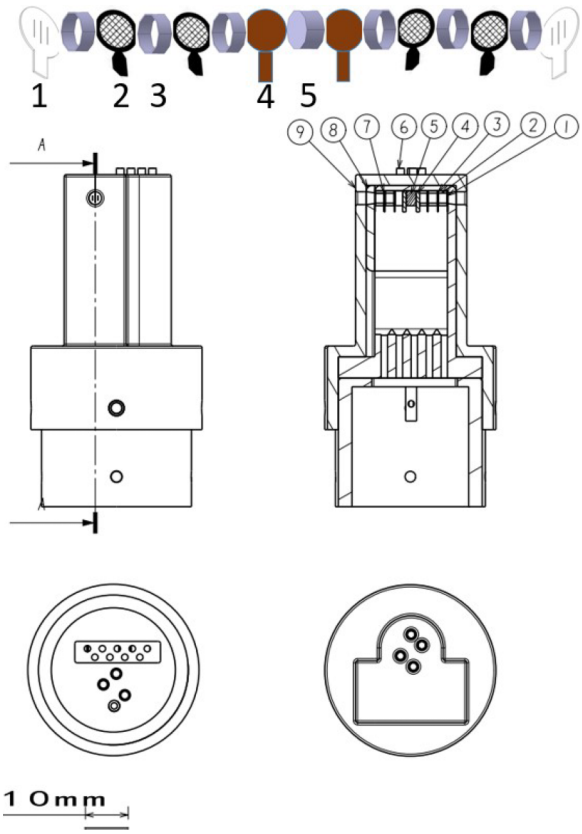

FIG. 2. Drawings of the EAST RFA probe head. No. 1 represents the entrance slit, No. 2 the tubular spacer ring, No. 3 the grid, No. 4 the collector, No. 5 central spacer, No. 6 the Langmuir probe, No. 7 the ring for electrical contact, No. 8 the cavity, and No. 9 the graphite shield.

been chosen to be 30 ± 5 μm and 100 ± 10 μm, respectively. The spacing between the adjacent slits is 500 ± 10 μm. The lengths of the central slit and two side slits are 1500 ± 10 μm and 1150 ± 10 μm, respectively. The transmission electron microscopy (TEM) grid from Ted Pella, Inc.[14] uses the RFA grid electrodes, being 3.05 mm of diameter and 35 μm of thickness. The optical transmission of the 75 mesh grid is 70%. Six contact rings of RFA are soldered to high temperature resistant cables inside the cavity. To insulate the adjacent solder joints, the distance between the two grids is maintained 2 mm using tubular ceramic spacers. The overall length of the ceramic cavity is 17 mm. The bi-directional RFA components are symmetrically installed in the cavity to measure the upstream and downstream ion temperature from the I-V curves and Mach number from the ratio of the ion saturation currents on the negatively biased entrance slit plates. The ceramic cavity is protected by the graphite shield. A picture of two RFA heads used in 2012 and 2016 campaigns and differed by the pin numbers (respectively one and four) of additionally incorporated Langmuir probe is shown in Fig. 3. Monitoring the sudden change in the floating potential near the last closed flux surface (LCFS) location allows for the control of the RFA slit position inside the plasma. During the 2016 campaign, the single probe was replaced by four-point probes to have a possibility to measure the electron density and temperature simultaneously. The ceramic ring as shown in Fig. 3 is used to connect the probe assembly to the rod to electrically insulate

FIG. 3. Photographs of the RFA assembly, where (a) was used during the 2012 campaign and (b) for the 2016 campaign.

the plasma from the ground. The RFA head can be quickly screwed to the probe shaft of a fast reciprocating probe system (FRPS).[15] Based on the sizes of small parts of the RFA head, the I_0 and I_{SCL} can be estimated according to Eqs. (4) and (8). It gives $I_0 = 2.2389 \times 10^{-5}$ A for $B = 1.7$ T, $T_i = 20$ eV, $n_i = 1.0 \times 10^{18}$ m^{-3}, $d = 2$ mm, $V = 190$ V, slit width $w = 30$ μm, height $h = 1500$ and 1150 μm, $\xi_r = 0.23$, $\xi = 0.3$, and M = 0.25. Taking into account that the width of the ion beam inside the RFA cavity is limited to $2\rho_i$ of Larmor radius, the I_{SCL} value is 1.033×10^{-4} A, being an order of magnitude larger than the estimated value of I_0.

C. RFA circuit design

The RFA has been operated with two entrance slits DC biased at $V_s = -150$ V to repel plasma electrons, positive scanning AC voltage V_G = 0-200 V on the first grid to discriminate the ions, and DC $V_{G2} = -190$ V on the second grid to suppress secondary electrons from the collector. The collector was connected to the chamber wall through a current-to-voltage conversion resistance. A sketch of the RFA circuit is shown in Fig. 4. Each signal is transmitted by the 25 m coaxial cables to electronic circuits isolated by optoelectronic isolators, from the data acquisition (DAQ) system. The electronics converts the currents of the order of milliamperes to the voltages inside ±5 V of DAQ voltage range. The DC bias was provided by the 9 V battery packs. The sweep voltage was obtained from the 50 Hz wall-plug power using a variable isolation transformer and rectifier bridge resulting in the sweeping frequency of 100 Hz. The values of sampling resistances in Fig. 4 are $R_{ES} = 8.2$ Ω, $R_{G1} = R_{G2} = 1$ kΩ, $R_C = 8.2$ kΩ, $R_2 = 200$ kΩ and $R_1 = 2$ kΩ.

With the circuit in Fig. 4, the ion saturation currents, required for the estimation of the plasma flow velocity, are measured on the negatively biased RFA slit plates. The ratio of the ion saturation currents, j^u_{sat} and j^d_{sat}, from the oppositely oriented upstream/downstream (u/d) RFA slits determines the Mach number $M = v_i/c_s$ (being c_s the ion sound speed) as[16]

$$M = 0.4 \ln\left(\frac{j^u_{sat}}{j^d_{sat}}\right). \tag{9}$$

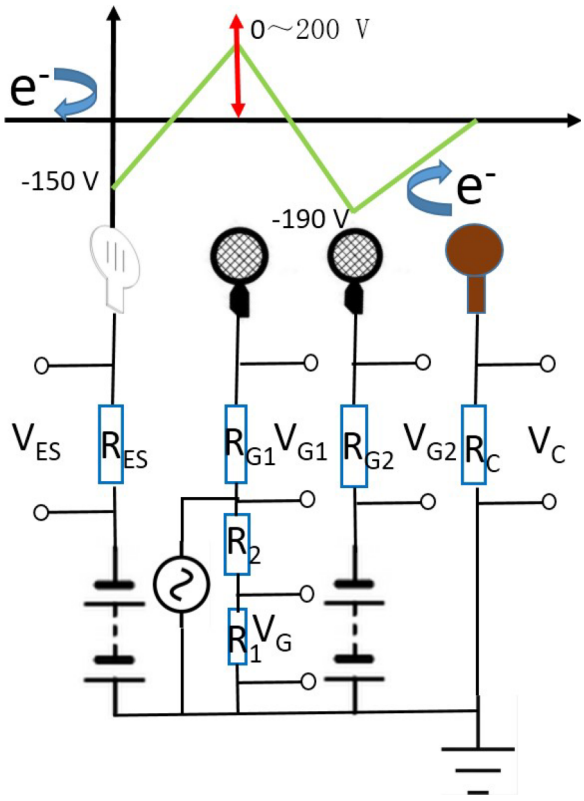

FIG. 4. Schematic diagram of the bias potential arrangements for an RFA operated in the ion collection mode and the corresponding circuit diagram.

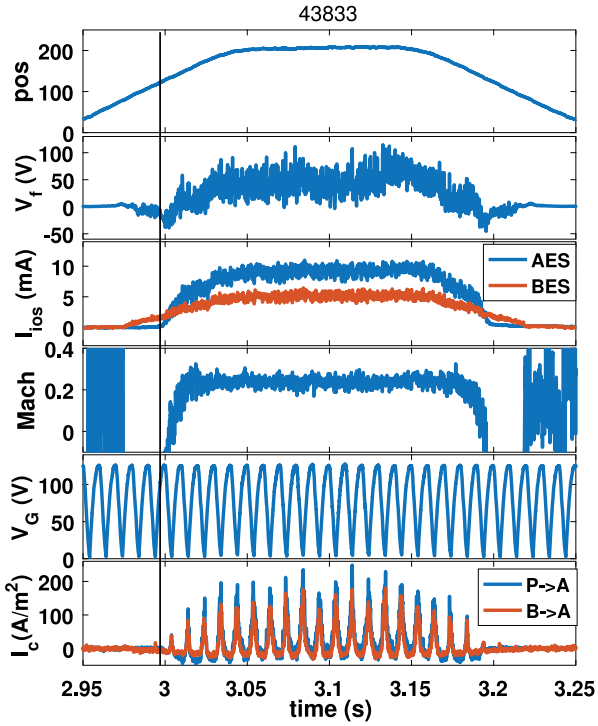

FIG. 6. RFA signals from a discharge (No. 43833), where pos is the RFA head insertion distance, V_f the floating potential, I_{ios} the ion saturation current, M the Mach number, V_G the scanning voltage, I_c the collector current, AES and BES refer to the ion and electron drift sides of the bidirectional RFA. P → A and B → A indicate the direction from port P to port A and from port B to port A, respectively. The black line indicates the turn-on point.

III. RESULTS

A. Ion temperature

It should be noted that generally the RFA can be installed in different diagnostic ports of EAST, distributed as shown in Fig. 5. Particularly, the typical RFA signals from port A together with the signals of RFA position (pos), floating potential (V_f), ion saturation current (I_{ios}), and Mach number are shown in Fig. 6 for limiter Ohmic discharge #43833. In Fig. 6 AES and BES marks indicate the ion and electron drift sides of the bi-directional RFA (the respective relative directions of P → A and B → A ports).The probe is moved forward into the plasma for 200 mm within 100 ms and stayed there for 100 ms before being moved backward. The temporal evolution of the collector current I_c is modulated by the retarding voltage V_G in grid 1. When the RFA head was inserted deep enough into the SOL, the ion saturation current from the RFA facing the ion drift side, AES is larger than that facing the electron drift side, BES. Because the poloidal limiter is located between P and A ports, the turn-on point (the time at which the RFA entrance slit currents become visible) of AES signal is lagged behind BES's signal (vertical black line in Fig. 6), effectively indicating the radial position of the leading edge of the poloidal limiter. Using this indication, the radial profiles of the Mach number and T_i are plotted in Fig. 7. From Fig. 7(a) the Mach number is nearly constant inside the separatrix, reaching $M = 0.25$ between the radii of $\Delta_r = -80$ mm and $\Delta_r = -20$ mm, while the T_i profile shown in Fig. 7(b) gradually increases as the RFA head is inserted deeper into the core plasma. The negative offset of the I_c can be caused by the outgassing of the poloidal limiter and breakdown-like processes inside the RFA cavity. The asymmetric of the negative current of I_c between P → A and B → A at the highest V_G when the RFA entered and left the SOL region (shown in Fig. 6) is possibly caused by the outgassing of the poloidal limiter which is located between ports P and A since the negative offset in P → A direction is

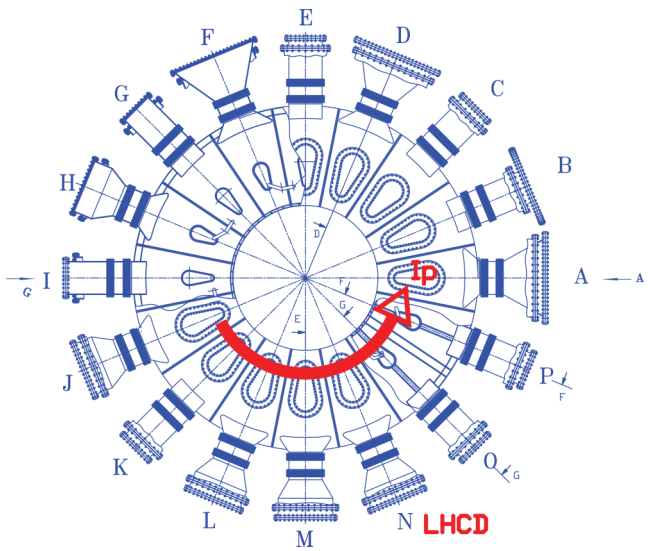

FIG. 5. The top view of the EAST where LHCD is located at N port. The plasma current Ip is along counter-clockwise direction.

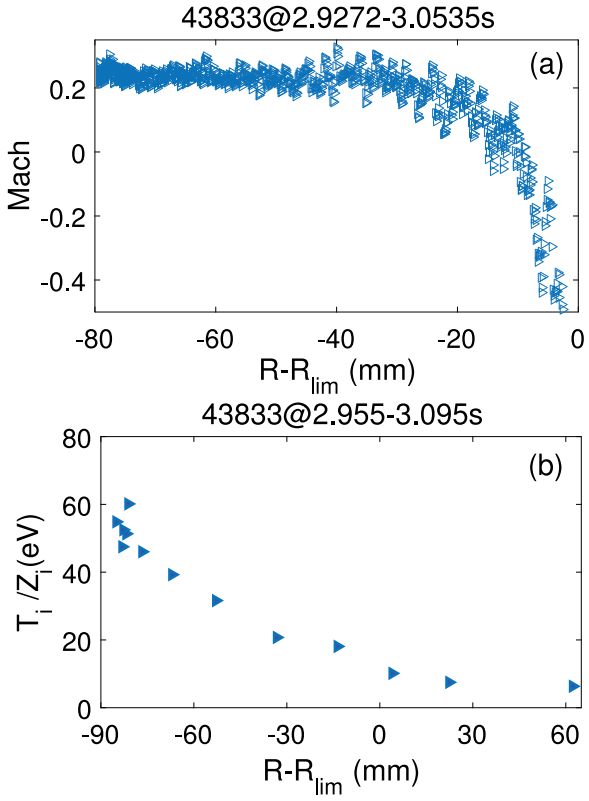

FIG. 7. (a) Mach number profile and (b) ion temperature profile where the temperature shown is the mean of the temperatures measured by RFAs in the electron and ion sides.

larger than the one of B → A direction. Note that the T_i profile in Fig. 7 flattens near the leading edge of the poloidal limiter.

B. Fast electron flux during LHCD

During LHCD operation, RFA has measured a strong fast electron flux passing the entrance slit and impacting on the collector. This collected fast electron flux is attributed to the lower hybrid wave (LHW) driven fast electrons by Landau damping in the SOL.[17] Since the fast electron flux is driven along the magnetic field lines, RFA will only measure the unidirectional value when it is plunged into the plasma. During the 2012 campaign, RFA located at port A has measured the fast electron flux in the ion side, AES. The electron side, BES, still measured the ion temperature. The direction of plasma current was in the counterclockwise direction, Fig. 5. In discharge #44255, with the LHCD power of 1.7 MW and $\langle n_e \rangle = 1.8 \times 10^{19}$ m^{-3}, the measured fast electron flux was ~2 kA/m^2 2 cm inside from the leading edge of the poloidal limiter, Fig. 8(a). This current was attributed to the negative $n_{\|}$ part of LHW located at port N. During the 2014 campaign, RFA was mounted at port K and has measured fast electron flux in the electron drift side. In discharge #52692, with the LHCD power of 0.6 MW, and $\langle n_e \rangle = 1.6 \times 10^{19}$ m^{-3}, RFA has been pushed into SOL 4.5 cm inside from the leading edge of the poloidal limiter, and the value of fast electron flux in the electron drift side was ~1 kA/m^2 and increasing significantly near the separatrix, Fig. 8(b).

C. Fast electron during edge localized mode (ELM) events

In EAST discharges with L-H transition, the RFA inserted close to the separatrix (20 mm from the leading edge of the poloidal limiter) responses on the ELM events as shown in Fig. 9 for discharge #44261, with the LHCD power of 1.7 MW, ion cyclotron resonance frequency (ICRF) power of 1.4 MW, and $\langle n_e \rangle = 3.2 \times 10^{19}$ m^{-3}. During the ELM events, the RFA collector current in the ion drift side is negative and is as high as ~6 kA/m^2. The RFA collector current in the electron drift side is negative also, but a much smaller value of about ~1 kA/m^2. These observations indicate that during the ELM event, there are substantial amount of electrons with energy exceeding 150 eV in the SOL region. Pitts *et al.* observed a positive current on the collector of RFA in JET during the

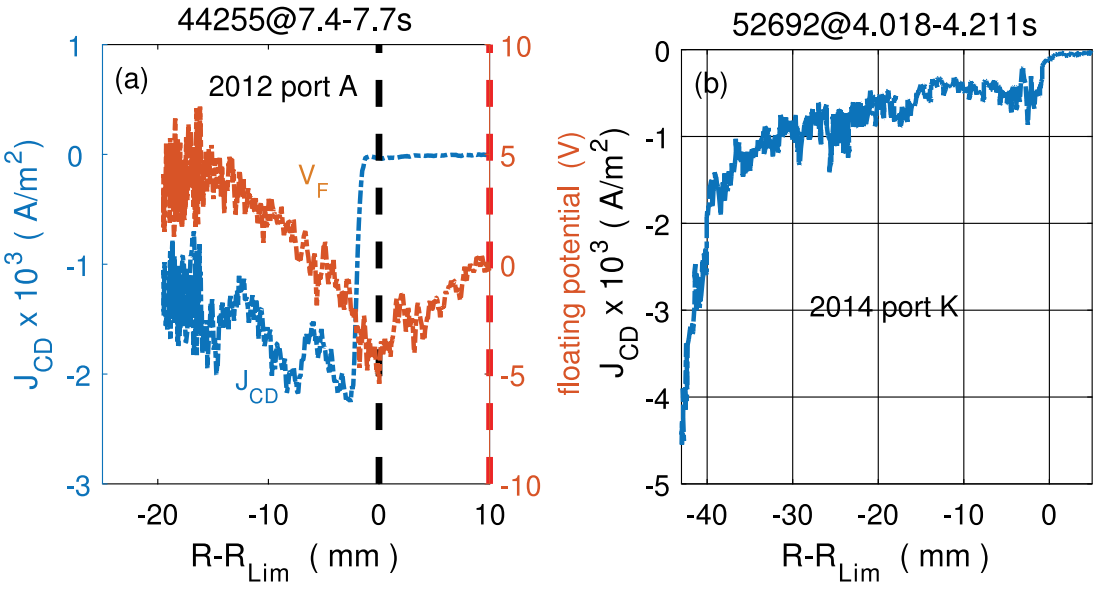

FIG. 8. (a) Fast electron flux in the ion side measured by RFA located at port A in the 2012 campaign; (b) fast electron flux in the electron side measured by RFA located at port K in the 2014 campaign.[17]

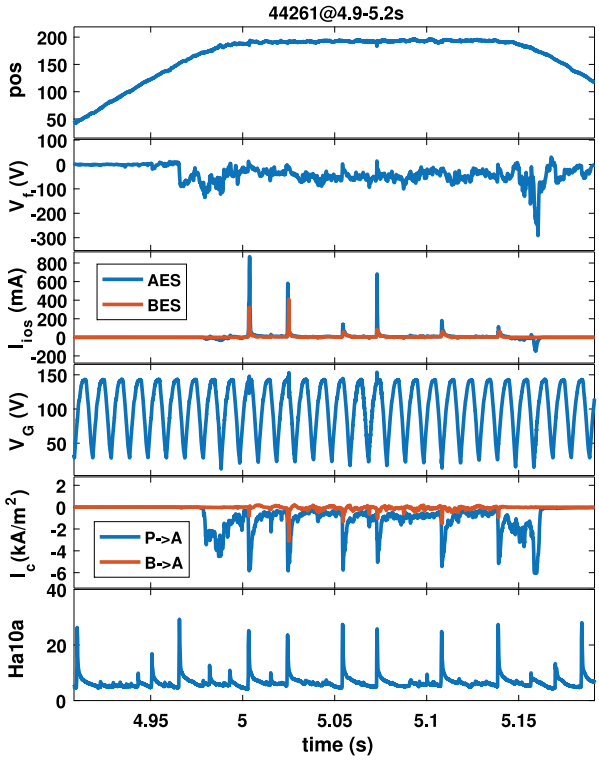

FIG. 9. RFA signals from a discharge (No. 44261). Note that the collector current both in ion and electron sides had negative spikes during the ELM events.

ELM events.[18] The negative current observed in EAST in the ion drift side can be related to the fast electron flux driven by LHCD which interacts with the hot plasma carried by ELMs to the SOL region. But the negative current in the electron drift side in EAST is opposite to the JET result of positive current. The difference may be linked to the different heating methods and power levels in the two devices. The auxiliary heating power during shot #44261 in EAST was 1.7 MW LHCD in addition to 1.4 MW ICRF, while in JET the heating power during shot #63214 reported in Ref. 18 was 4.5 MW neutral beam injection (NBI) and 2 MW ICRF. Since the filaments during the ELM events carry pedestal plasma with fast electrons produced by LHCD and transport to SOL, the negative current in the electron drift side may be from the pedestal region.

IV. SUMMARY

A bidirectional RFA probe has been developed for EAST to measure the ion temperature and fast electron fluxes in both ion and electron drift sides. A four-pins probe assembly has been added on the top of the RFA head to control the RFA position relative to the LCFS and to measure the electron density and temperature. The ion temperature profile has been measured by RFA in the SOL of Ohmic plasmas. RFA has also measured the strong fast electron fluxes entering the entrance slit and impacting on the collector in both ion and electron drift sides in LHCD discharges. The value of fast electron flux in the electron side is ~1 kA/m^2 increasing significantly near the separatrix. Substantial fast electron flux has been also measured by RFA during the ELM events in discharges with L-H transition. The results showed that the fast electron flux in the ion drift side is larger than that in the electron drift side. Comparing with the fast electron flux measured by RFA in L mode and in inter-ELM period, the fast electron flux during the ELM event can be produced by LHCD interacting with hot plasma carried through ELMs into SOL. Furthermore, as LHCD drives the dominant current in EAST tokamak, fast electrons would exist not only in the SOL but also in the main plasma region. It is plausible to speculate that the fast electrons measured by the RFA collector in the electron drift side came from the pedestal region.

ACKNOWLEDGMENTS

The support from E. Z. Li, J. P. Qian, S. Ding, L. M. Shao, H. Lan, N. Zhao, Q. Q. Yang, H. Liu, Y. F. Wang, Q. Wang, and the EAST team is greatly acknowledged. This work is supported by the National Magnetic Confinement Fusion Research Program of China under Contract Nos. 2015GB101000 and 2015GB101002, and the National Natural Science Foundation of China under Grant Nos. 11422546, 11405212, and 11405213.

[1]J. A. Simpson, Rev. Sci. Instrum. **32**(12), 1283 (1961).
[2]D. Brunner, B. LaBombard, R. Ochoukov *et al.*, Plasma Phys. Controlled Fusion **55**(12), 125004 (2013).
[3]R. A. Pitts, R. Chavan, S. J. Davies *et al.*, Rev. Sci. Instrum. **74**(11), 4644–4657 (2003).
[4]M. Kočan, J. P. Gunn, M. Komm *et al.*, Rev. Sci. Instrum. **79**(7), 073502 (2008).
[5]D. Brunner, B. LaBombard, R. Ochoukov, and D. Whyte, Rev. Sci. Instrum. **84**(3), 033502 (2013).
[6]I. S. Nedzelskiy, C. Silva, and H. Fernandes, Rev. Sci. Instrum. **85**(9), 093506 (2014).
[7]M. Dreval, D. Rohraff, C. Xiao, and A. Hirose, Rev. Sci. Instrum. **80**(10), 103505 (2009).
[8]K. Kreuger, Z. H. Huang, M. Jiang *et al.*, Radiat. Eff. Defects Solids **168**(10), 776–788 (2013).
[9]J. P. Gunn, V. Petržílka, A. Ekedahl *et al.*, J. Nucl. Mater **390–391**, 904–906 (2009).
[10]J. P. Gunn, V. Fuchs, V. Petržílka *et al.*, Nucl. Fusion **56**(3), 036004 (2016).
[11]M. Kočan and J. P. Gunn, Plasma Phys. Controlled Fusion **53**(8), 085016 (2011).
[12]R. J. Umstattd, C. G. Carr, C. L. Frenzen *et al.*, Am. J. Phys. **73**(2), 160 (2005).
[13]See http://www.gatewaylaser.com/ for information about laser drilling.
[14]See https://www.tedpella.com/grids_html/Pelco-TEM-Grids.htm for information about mesh grids.
[15]W. Zhang, J. F. Chang, B. N. Wan *et al.*, Rev. Sci. Instrum. **81**(11), 113501 (2010).
[16]I. H. Hutchinson, Phys. Fluids B **3**, 847 (1991).
[17]Y. L. Li, G. S. Xu, H. Q. Wang *et al.*, Phys. Plasmas **22**(2), 022510 (2015).
[18]R. A. Pitts, W. Fundamenski, S. K. Erents *et al.*, Nucl. Fusion **46**(1), 82–98 (2006).